Shell-side dispersion coefficients in a rectangular cross-flow hollow fibre membrane module

Dindore, V. Y.; Cents, A. H. G.; Brilman, D. W. F.; Versteeg, G. F.

Published in:
Chemical Engineering Research and Design

DOI:
10.1205/cherd.04166

Publication date:
2005

IChemE

www.icheme.org/journals
doi: 10.1205/cherd.04166

0263–8762/05/$30.00+0.00

Trans IChemE, Part A, March 2005
Chemical Engineering Research and Design, 83(A3): 317–325

SHELL-SIDE DISPERSION COEFFICIENTS IN A RECTANGULAR CROSS-FLOW HOLLOW FIBRE MEMBRANE MODULE

V. Y. DINDORE[1,*], A. H. G. CENTS[1], D. W. F. BRILMAN[2] and G. F. VERSTEEG[1]

[1]*Design and Development of Industrial Processes, Faculty of Chemical Technology, University of Twente, P.O. Box 217, 7500 AE, Enschede, The Netherlands*
[2]*Sasol Technology Netherlands B.V., P.O. Box 217, 7500 AE, Enschede, The Netherlands*

Membrane processes utilizing hollow fibre membrane modules are gaining increased interest in many industrial applications. However, these modules suffer from shell-side maldistribution and bypassing which results in a loss in efficiency. The shell-side mass transfer performance of these membrane modules strongly depends on the shell-side mixing and the shell geometry. In literature limited information is available on the shell-side mixing of hollow fibre membrane modules. In the present work, shell-side mixing of a rectangular cross-flow hollow fibre membrane contactor is investigated using gas-phase RTD measurements. A novel ultrasound based measurement technique was used to characterize the system. The shell-side mixing of the module is determined in terms of dispersion coefficients in three directions. The axial dispersion coefficient is found to have values between those applicable to pipe-flow and packed bed correlations. This can be attributed to the intermediate packing density of the membrane module. The dispersion in transversal directions, along and across the fibres, is significantly lower compared to that of the axial dispersion. The transversal dispersion coefficient across the fibre is higher and more sensitive to the shell-side velocity compared to the dispersion coefficient along the fibre due to the continuous splitting and remixing of shell-side flow across the fibres.

Keywords: membrane contactor; dispersion model; RTD; mixing; hollow fibre membranes.

INTRODUCTION

Polymeric hollow fibre membrane modules have gained widespread use in process industry for various purification and recovery processes and are being increasingly important in medicinal field as artificial kidneys and lungs. In addition, due to the unparallel advantages offered by these modules, considerable academic as well as industrial work has been done to apply these modules for non-dispersive contacting of the gas and liquid phases. Common hollow fibre membrane modules consist of hair-like hollow fibres potted at both ends and installed in various shell geometries. The performance of these membrane modules is often characterized by how efficiently a module separates the components from a mixture. Prediction of the module performance for design purpose requires knowledge of the mixing patterns and mass transfer characteristics on the shell-side, lumen-side and of the membrane. The lumen side flow pattern and mass transfer are generally well described using the heat transfer analogy (Skelland, 1974). The membrane mass transfer properties are typically available from the membrane manufacturer or can be determined using simple experiments (Mulder, 1996). In contrast to lumen side flow, shell-side flow is not clearly understood and scarce information is available for predicting shell-side mixing patterns and mass transfer characteristics. Moreover, the shell geometry strongly influences the shell-side mass transfer performance and different shell geometries are used depending on various factors such as process requirements, equilibrium considerations, availability of membrane materials and mass transfer limitations etc. In general, the use of cross-flow configuration in membrane contactors is favoured because a considerable enhancement in the shell-side mass transfer coefficient can be obtained by positioning the membrane fibres perpendicular to the flow direction (Wickramasinghe *et al.*, 1992). In addition, cross-flow membrane modules offer reduced shell-side maldistribution and lower pressure drop compared to that of parallel flow modules (Feron *et al.*, 1994).

Typical approaches for predicting the shell-side mixing behavior and the mass transfer performance either require solving the continuum mass and momentum balances based on first principles, relying on completely empirical correlations or using a model which contains few empirical

*Correspondence to: Dr V. Y. Dindore, Chemical Engineering Department, NTNU, N-7491, Trondheim, Norway.
E-mail: vishwas.dindore@chemeng.ntnu.no

parameters and approximates the actual behaviour closely. The first approach would require the descretization of the complex three dimensional (3D) geometry and solving the large sets of computationally demanding equations. However, in many cases it is possible to assume simplified flow patterns. This approach is possible in more simple geometries, e.g., parallel flow in shell and tube geometry without baffles. In such cases, many researchers have assumed a simplified geometry of flow around a single fibre and Happel's free surface model (Chun and Lee, 1997; Karoor and Sirkar, 1993). However, these simplifications do not match with the real module performance due to uneven distribution and bending of fibres (Kreulen *et al.*, 1993). Moreover, in the case of the cross-flow contactor such simplification of flow pattern would result in inaccurate description of the module performance due to the continuous splitting and remixing of the shell-side phase. The second approach is to derive empirical correlations to predict the mass transfer performance without knowing the details of mixing behaviour. The experimentally derived correlations are strongly influenced by the module geometry used, and are specific for the flow configuration. Moreover, these correlations are subjected to suffer from channeling effects, polydispersity and uneven distribution of the fibres (Dahuron and Cussler, 1988; Wickramasinghe *et al.*, 1992).

The third approach is intermediate between the first two approaches. In this case, the valuable information on the macroscopic mixing behaviour of the phase flowing through a reactor is obtained, without knowing the exact flow patterns, by measuring the deviation of the flow from the two ideal flow patterns; namely ideally mixed and completely plug flow. This information on the hydrodynamics is then incorporated in the reactor model. These semi-empirical models have been successfully used to describe the flow system in various industrial contactors. Thus the determination of the macroscopic mixing behaviour on the shell-side of a membrane module is of significant importance. Generally, this information is deduced from the measurement of the residence time distribution (RTD), and fitting a model to represent a real process which has the same or a similar type of the residence time distribution. In the present work, shell-side hydrodynamics of the rectangular cross flow hollow fibre membrane contactor is investigated using RTD measurements. For the experimental simplicity and to avoid the bending of fibre due to high shear of the fluid flowing perpendicular to the fibre, gas phase tracer response is selected to study the residence time distribution in the rectangular cross-flow hollow fibre membrane module.

ULTRASONIC RTD MEASUREMENT TECHNIQUE

Measurement Principle

Various RTD measurement techniques are reported in literature. For accurate measurements the technique needs to be non-intrusive, causing minimum flow disturbances and, for the present case, should be capable of measuring residence times in the range of 0.1 s. Most reported techniques for single-phase RTD measurements are based on (laser) light transmission (Nadeau *et al.*, 1996), thermal conductivity (Brereton *et al.*, 1988) or radioactive tracers (Viitanen, 1993). For single-phase systems all these methods can be applied with good performance characteristics and at high sampling frequencies. Disadvantages of light-based techniques are their inability to measure through non-transparent reactors and reactor walls. Thermal conductivity can only be applied with intrusive probes, which is undesired because of the disturbance of the flow-pattern. From the abovementioned techniques only the radioactive tracer-gas method meets all requirements, but requires extensive safety procedures. In this study, a novel gas-phase RTD measurement technique based on the dependence of the ultrasonic velocity on the gas-phase composition is used (Cents, 2003). The method meets all the requirements and, in addition, offers the opportunity to measure through nontransparent reactor walls.

In this section, the principle of the measurement technique will be explained briefly and the method will be validated for a single phase ideal plug flow (PFR) and completely mixed (CSTR) reactors for short holding times. Subsequently, the RTD measurements and its analysis for the rectangular cross-flow hollow fibre membrane contactor using this novel method will be presented.

The measurement principle of this novel method makes use of the dependence of the speed of sound in a material on the bulk modulus (of elasticity) and density of the medium. This dependence for a pure component by equation (1) (Povey, 1997).

$$v = \sqrt{\frac{dp}{d\rho}} = \sqrt{\frac{E_v}{\rho}} \tag{1}$$

Both the density and the bulk modulus of the pure components used in this study (helium and nitrogen) are well tabulated in the literature or can be accurately estimated (Povey, 1997). Equation (1) is also applicable for a mixture of gas (e.g., air), however in such cases corresponding values density and bulk modulus of elasticity of the mixtures should be used. The average density and bulk modulus of a binary mixture of ideal gases are given by:

$$\rho = (1 - \phi)\rho_1 + \phi\rho_2 \tag{2}$$

where, ϕ is the volume fraction of component '2'.

$$\frac{1}{E_v} = (1 - \phi)\frac{1}{E_{v,1}} + \phi\frac{1}{E_{v,2}} \tag{3}$$

Thus using equations (1), (2) and (3), the composition of the binary mixture can be expressed as function of the measured velocity of sound in the mixture and the known ρ and v values of the pure components:

$$\phi = \frac{-B \pm \sqrt{B^2 - 4AC}}{2A} \tag{4}$$

where

$$A = v_1^2\left(1 - \frac{\rho_1}{\rho_2}\right) + v_2^2\left(1 - \frac{\rho_2}{\rho_1}\right) \quad (4a)$$

$$B = v_2^2\left(\frac{\rho_2}{\rho_1} - 2\right) + v_1^2\frac{\rho_1}{\rho_2} \quad (4b)$$

$$C = v_2^2\left(1 - \frac{v_1^2}{v^2}\right) \quad (4c)$$

Equation (4) was used to convert the experimentally determined sound velocity values into the mixture's composition. Note that, in the above analysis, the term binary is not restricted to two pure components. The relation also holds when a component, the tracer-gas, is considered with a mixture of components (e.g., air) whose relative composition does not change during the measurement. This concentration measurement technique can be used to determine the system's response to a step-function as well as to measure steady state local concentration gradients. Thus, this technique also provides an opportunity to measure the radial concentration profile.

Determination of the Velocity of Sound

The velocity of sound is determined using a tone-burst technique. A tone-burst is a narrow banded signal consisting of a certain number of periods of a single frequency. The velocity of this signal is measured as the path length divided by the time of flight (TOF) of the signal from the transmitting transducer to the receiver one. The TOF is difficult to determine directly, because the transfer function of the complete measurement system is not known. For this reason the time difference (Δt) is determined between the signal in the mixture and a reference signal in which the velocity of sound is known accurately (e.g., in air). The velocity of sound in air (v_r) is taken from the CRC's Handbook of Chemistry and Physics (1999). From these values the velocity of sound in an unknown medium can be calculated as:

$$v = \frac{x}{t} = \frac{x}{(x/v_r) + \Delta t} \quad (5)$$

The path length (x) in the measurement cell can be determined with an accurate caliper or by the measurement of the time difference (Δt in equation (5)) between a reference signal in air (which has travelled once the path length) and its first reflection (which has travelled three times the path length).

EXPERIMENTAL

The experimental set-up consists of an arbitrary waveform generator (AWG), which sends any desired electric signal to a piezo-electric transducer (T) with a centre frequency of 800 kHz. The signal is amplified with a maximum of 44 dB with a variable power amplifier. The transmitting transducer converts the electric signal to a pressure wave that is received at another transducer (R). The converted electric signal is, after 31 dB amplification, acquired with a maximum sampling rate of 2 GS/s (2×10^9 samples per second) and with 8-bits resolution in a digital oscilloscope. At the same time as the AWG sends the electric signal, a trigger signal is transmitted both to the oscilloscope and to an electrically controlled valve to start tracer injection. In this way in every measurement the starting point, $t = 0$, is well defined. Data from the oscilloscope is transferred to the computer using a GPIB interface bus. The overall sampling frequency in this experimental set-up is limited by the data transfer rate and is 33 Hz. Although this inadequacy could be eliminated by approaching the theoretical maximum sampling frequency in the order of 10,000 Hz, the current system was found to be sufficiently accurate. The complete set-up is schematically represented in Figure 1. The measurement cell is made of two transducers one for transmitting the signal and other for receiving it. The measurement cell can be placed at several locations in the reactor with out disturbing the flow pattern of the reactor. Both the input step function as well as the response leaving the reactor could be measured in this way. The path length applied in the measurement was 18 mm, and the cell was designed to minimize the disturbance of the flow in the employed reactors. Helium was selected as the tracer-gas because of its pronounced difference in sound velocity compared to N_2 (983 m/s vs. 345 m/s at 23°C). N_2 was introduced in the reactors through a mass flow controller and the total outgoing flow rate was derived from the N_2 flow-rate and the total helium fraction.

To validate the accuracy of the technique in general and to test its applicability at low residence times, experiments were carried out using reactors with nearly ideal flow patterns with low residence times. A reactor vessel with a volume of 1220 ml equipped with a magnetic stirrer was used to imitate the ideally mixed gas-phase flow pattern (CSTR). In addition, two stainless steel tubular reactors with inner diameters of 19.0 mm and 18.4 mm and lengths of 1635 mm and 815 mm, respectively, were used to approximate plug-flow (PFR) behaviour ($Pe > 50$). To study the shell-side mixing behaviour of cross-flow hollow fibre membrane contactors, experiments were carried out using a commercially available module, provided by TNO-MEP, Apeldoorn. The module was made up of microporous polypropylene hollow fibres (Accurel PP: Type Q3/2; inside diameter 600 μm; wall thickness

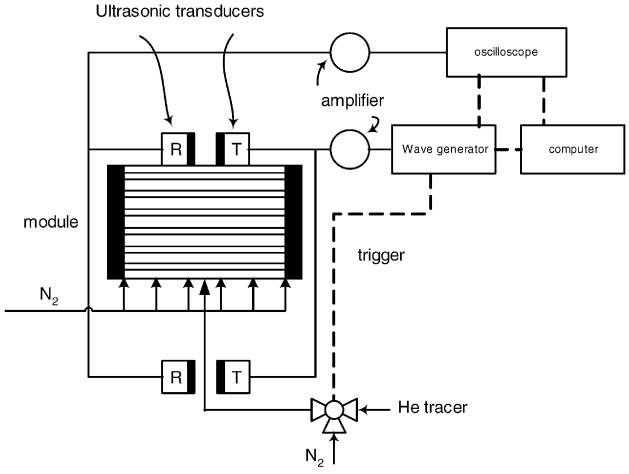

Figure 1. Experimental set-up RTD analysis of membrane module.

200 μm). The module was 0.1 m × 0.1 m × 0.1 m (H × W × L) in dimensions and contained around 4900 fibres arranged in in-line square pitch (pitch = 1.45).

Two different sets of experiments were carried out to study the mixing in all three directions, i.e., in the direction of the gas flow, in the directions perpendicular to the gas flow (along and across the fibres) respectively. Initial experiments were performed to determine the axial mixing (in the direction of the gas flow) in terms of an axial dispersion coefficient (E_z). To determine the axial dispersion coefficient, a step input of the tracer was given and its response at the exit of the module was measured as function of time. The measurement cells were located 11 cm after the module outlet and 35 cm before the module inlet. The dead time due these measuring tubes was taken into account in the calculations.

The next set of experiments was aimed at the determination of dispersion coefficients (E_x, E_y) in the transversal or normal to the flow direction. In this case, the tracer was introduced as a point source at a known inlet location into the module. The velocity of the tracer was kept same as the velocity of nitrogen flow in the rest of the module. The steady state concentration profile of the tracer was determined at the exit of the module by measuring the concentration of the tracer at various positions in the 'x' and 'y' direction. A perforated plate with 8 × 8 grid holes was used to change the position of the measuring cell in the top x–y plane of the module.

Since the fibres used in the module are microporous, accumulation of the tracer gas inside the fibres might occur. To avoid this tracer gas accumulation, the fibres in the module were filled with the water during all experiments.

INTERPRETATION OF RTD MEASUREMENTS

Axial Dispersion Coefficient

This section focuses on the employed methods/models for the interpretation of the concentration response curves to estimate the axial dispersion coefficient. The residence time distribution, which is essentially a statistic description of the fluid flow, expresses the probability of an entering fluid element to leave the reactor after a certain time. It is common practice to use the probability function, E, to describe the distribution of residence times:

$$\int_0^\infty E(t)\,\mathrm{d}t = 1 \tag{6}$$

The cumulative function, F, is also frequently used for the representation of the RTD:

$$F(t) = \int_0^t E(t)\,\mathrm{d}t \tag{7}$$

The mean residence time (first moment) can be calculated on basis of the E- and F-curve as follows:

$$\bar{t} = \int_0^\infty t\,E(t)\,\mathrm{d}t = \int_0^1 t\,\mathrm{d}F(t) \tag{8}$$

This equation provides the most direct method for the calculation of the mean residence time. It is interesting to compare the mean residence time derived from the RTD experiments with the holding time (τ) calculated by dividing shell-side volume by the shell-side volumetric flow rate. This comparison will yield information regarding the presence of dead-zones and/or bypass streams with hardly any exchange to the main flow field.

Normally the F-curve is presented using a reduced time (θ).

$$\theta = \frac{t}{\tau} \tag{9}$$

The spread in residence time is characterized by the variance:

$$\sigma^2 = MO_2 - (\bar{t})^2; \quad \sigma_\theta^2 = \frac{\sigma^2}{\tau^2}; \quad N = \frac{1}{\sigma_\theta^2} \tag{10}$$

where

$$MO_2 = \int_0^\infty t^2 E(t)\,\mathrm{d}t = 2\int_0^\infty t[1 - F(t)]\,\mathrm{d}t$$

In this work a step function was used as input function, which yields the F-curve as a response curse. The RTD-curves obtained were interpreted in three ways.

(a) The first method involve a model consisting of a cascade of N equal mixed tanks. A numerical fit-procedure was used to minimize the deviation between the measured F-curve and the model. Assuming an ideal input step, the analytical solution for this model is:

$$F(\theta) = \int_0^\theta \frac{N^N \theta^{N-1}}{(N-1)!}\mathrm{e}^{-N\theta}\,\mathrm{d}\theta = \frac{\Gamma_{\mathrm{in}}(N, N\theta)}{\Gamma(N)} \tag{11}$$

where

$$\Gamma(x) = \int_0^\infty u^{x-1}x^{-u}\mathrm{d}u$$

$$\Gamma_{\mathrm{in}}(x, y) = \int_0^y u^{x-1}\mathrm{e}^{-u}\mathrm{d}u$$

(b) In second method, the interpretation was carried out using the axially dispersed plug flow model using Danckwerts (closed–closed) boundary conditions at inlet and outlet respectively. The analytical F-curve for this case is given by equation (11) (Danckwerts, 1953).

$$F(\theta) = 0.5\left\{1 - erf\left(0.5\sqrt{Pe}\,\frac{(1-\theta)}{\sqrt{\theta}}\right)\right\} \tag{12}$$

In this method also, a numerical fit-procedure was used to minimize the deviation between the measured F-curve and the model. The resulting fit parameters are the mean residence time and the Peclet number relating the axial dispersion coefficient.

(c) In third approach, the RTD response of the system was interpreted directly on the basis of the F-curve using equations (8) and (10) to obtain $\bar{t}$ and N.

Transversal Dispersion Coefficients

When the information necessary to describe the flow pattern in a reactor is not known, a model which contains empirical parameters and approximates the actual flow behaviour is used to describe the mixing in the reactor. One of the most widely used models is the dispersion model. The general mathematical expression for this model is given by equation (13) for the case of a rectangular module with flow in z-direction.

$$\frac{\partial C}{\partial t} = E_x \frac{\partial^2 C}{\partial x^2} + E_y \frac{\partial^2 C}{\partial y^2} + E_z \frac{\partial^2 C}{\partial z^2} - \langle v \rangle \frac{\partial C}{\partial z} \tag{13}$$

where, E_z is the axial dispersion coefficient in the direction of flow, E_x and E_y are transversal (normal to the direction of flow) dispersion coefficients in x and y directions and $\langle v \rangle$ is the average fluid velocity through the module. In the case of rectangular hollow fibre membrane module, the difference between E_x and E_y can be identified as one along the length of fibre and other normal to the fibre, respectively. These coefficients are assumed to be independent of concentration and position. The transversal dispersion coefficients can be estimated by experimentally measuring the steady state concentration gradient normal to the flow at the outlet of the module and comparing it with solution of equation (13). The dispersion model can be solved numerically as well as analytically for various boundary conditions under the steady state condition. However, the analytical solution using three dispersion coefficients in three directions is rather complex, hence it was decided to solve the model using a numerical technique under steady state conditions. The following boundary and initial conditions were used to solve the model using an implicit numerical method.

$$C = 0 \quad \text{at } t = 0 \quad \text{for any } x, y, z \tag{13a}$$

At the walls of module the flux of tracer is assumed to be zero.

$$\frac{\partial C}{\partial x} = 0 \quad \text{at } x = 0 \text{ and } x = X \quad \text{for any} \quad y, z, t \tag{13b}$$

$$\frac{\partial C}{\partial y} = 0 \quad \text{at } y = 0 \text{ and } y = Y \quad \text{for any} \quad x, z, t \tag{13c}$$

$$C = C_{\text{ini}} \quad \text{at } z = 0 \quad \text{for known } x, y \text{ and } t > 0 \tag{13d}$$

$$\frac{\partial C}{\partial z} = 0 \quad \text{at } z = Z \quad \text{for any} \quad x, y, t \tag{13e}$$

The concentration profile of the tracer was calculated at all positions in the module under steady state conditions using guessed values of the transversal dispersion coefficients. The computed concentration at the outlet of the module was then compared with the experimental concentration profile and the guess value was changed if necessary. Thus the optimized values of transversal dispersion coefficients were obtained using a Nelder–Mead simplex routine to minimize the deviation between the experimental and computed concentration profile.

RESULTS AND DISCUSSIONS

Validation of the Method

To validate the ultrasonic technique regarding the ability to determine the composition of a binary gas mixture, the helium fraction in air calculated from the measured ultrasonic velocity of the mixture using equation (4) was compared with the helium fraction of a known mixture. The latter was based on the readings of the mass flow controllers placed in the nitrogen and helium supply lines. The results are shown in Figure 2, from which it can be concluded that the ultrasound technique can be used to determine the composition of a binary gas mixture. Obviously, the nature of the components has to be known [ρ_i and v_i in equation (4)].

The quality of the input step function, which determined from the speed at which the valve opens, can be very important in analysing the RTD responses. An example of this input step function (with 10 cm tubing after the valve) is presented in Figure 3, from which can be seen that the valve opens very fast. However, the actual profile was difficult to determine, at least within the current maximum sampling frequency of 33 Hz. Although exact values for the variance of the valve opening (σ_v^2) cannot be determined, the variance that can be determined from this curve is maximally $5.4 \times 10^{-5}\ \text{s}^2$ ($\sigma_\theta^2 = 6.4 \times 10^{-3}$). For pipe-flow experiments at a high gas velocity and at short residence times such operation of the value can still be important. In this case, the $F(t)$ curve in the tube should be determined using deconvolution of the response at the outlet and the inlet. In all other experiments the assumption of an ideal input step function is justified.

Figure 4 shows a typical measured step-response (helium fraction detected by the measurement cell after a step change in the input helium fraction) of one of the used PFRs ($D_t = 19$ mm and $L = 1635$ mm). In Figure 4 also the best fit of the N_{CSTR}-interpretation model is plotted. It can be seen that a very good fit is obtained between the experimental response and the model.

To measure the applicability of the measurement technique at low residence times, RTD analysis of tubular plug flow reactors with different low residence times (τ)

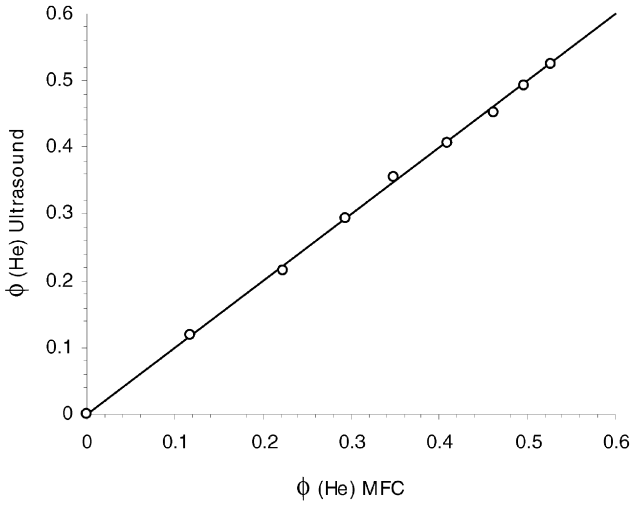

Figure 2. Parity plot of the volume fraction of helium calculated using equation (4) and according to mass flow controller readings.

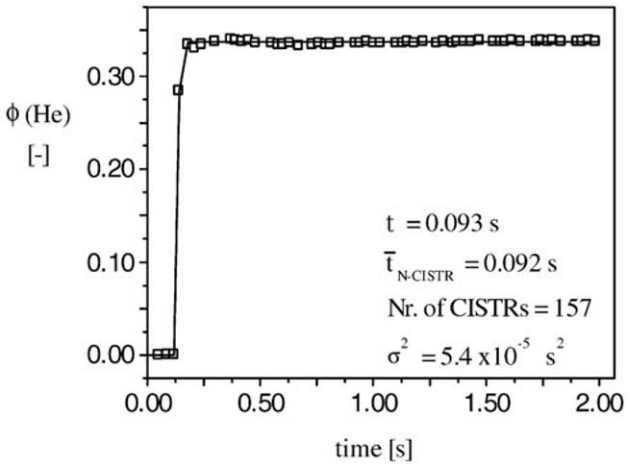

Figure 3. Response of the tracer injection valve.

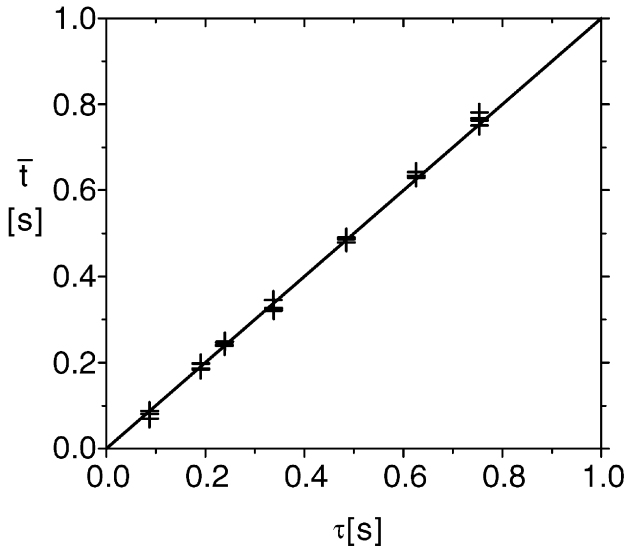

Figure 5. Parity plot of the mean residence time (calculated by interpretation of measured F-curve with the N_{CSTR}-model) and residence time of the PFRs.

was carried out. Figure 5 shows the mean residence time calculated from measured RTD-curves of the PFR versus the holding time. In this case, the RTD data were interpreted with the N_{CSTR}-model. Comparing the mean residence time calculated on basis of the F-curve, the axial dispersion model, and the N equal CSTR model never resulted in a deviation of more than 5% when a sufficiently high He-fraction (say 15%) was used. In case of lower He-fractions the noise level caused that direct integration of the raw F-curve became more difficult. Smoothening of the data by spline interpolation solved this problem.

Figure 5 clearly shows that this prototype of the measurement system is already able to determine the gas-phase RTD of reactors with a holding time down to 0.08 s. Note, that, according to the Nyquist theorem (Oppenheim and Schafer, 1989), only frequencies of less than 16.5 Hz can be reconstructed with the present sampling frequency (33 Hz). In principle using the current measurement cell with the theoretical maximum sampling frequency 10000 Hz, even systems with much smaller residence times can be analysed when the problem of data transfer is solved. However, for very short holding times (say $\tau < 0.05$ s) the dynamic behaviour of the tracer-gas injection valve may become dominant, and the input step must be determined in these cases. In general, a higher sampling frequency will improve the accuracy of the RTD-curve analysis, because more data are available on the slopes of the curves.

It was found that the use of standard dispersion model, as a data interpretation model, does not influence both the accuracy of the fit and the information obtained from the fit. In fact, for all responses both models were used, and it turned out that the approximate equation (for $Pe > 10$): $Pe/2 \approx N_{CSTR} - 1$ was always satisfied within 10%. The experimentally found Bodenstein numbers (range 0.6–3.0) were in good agreement with values according to the correlations given in literature for single-phase turbulent fluid flow in tubes (Wen and Fan, 1975).

Figure 6 shows a typical step-response of the CSTR. Also for the CSTR the mean residence time was in good

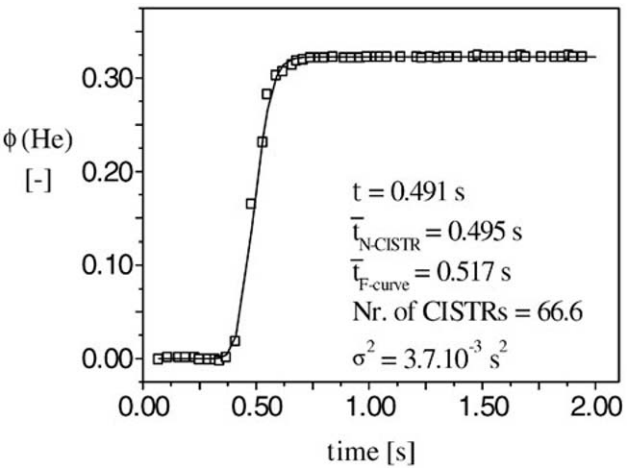

Figure 4. Typical step-response of one of the used PFRs. Experimental data and the best-fit line (N_{CSTR}-model) are plotted.

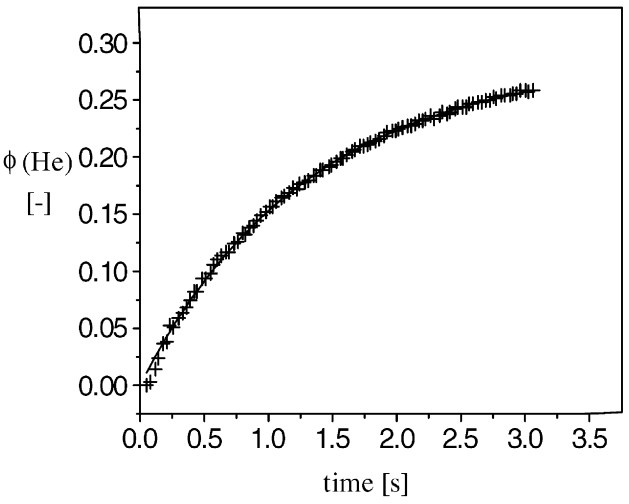

Figure 6. Typical step response of the CSTR. Experimental data and the best-fit line (N_{CSTR}-model) are plotted.

agreement with the holding time. Several RTD-curves were obtained: the number of CSTRs calculated varied between 0.9 and 1.1, indicating that the CSTR actually can be regarded as a CSTR.

On basis of the results described above it is concluded that the ultrasound method satisfies the demands for the measurement of the gas-phase RTD of single-phase reactors.

Analysis of the Cross-Flow Hollow Fibre Membrane Contactor

A typical F-curve in the RTD analysis of the rectangular membrane module is shown in Figure 7. It can be seen that the shell-side flow is neither resembles ideal plug flow nor can be regarded as a completely mixed cell. This indicates that there is significant mixing in the axial direction of the hollow fibre membrane module. Similar observations in the case of parallel flow hollow fibre membrane contactors were made by Wang *et al.* (2003). As indicated by these authors the non-ideal flow on the shell-side of module can seriously affect the mass transfer performance of the module. In a tracer analysis of commercial membrane extractor Seibert *et al.* (1993) found that significant bypassing of the shell-side fluid was present in the case of hollow fibre parallel flow modules. This was indicated by 3–4 times faster experimental residence time as compared to that of the holding time of the module. From the evenly placed age distribution around the holding time (corresponding to the residence time of PFR) in Figure 7, it can be concluded that such a strong bypassing of the shell-side fluid is absent in the case of cross flow hollow fibre modules. These F-curves were obtained for different velocities to study the effect of shell-side velocity on the dispersion coefficient. The axial dispersion coefficients were obtained by fitting equation (12) to the experimentally obtained concentration versus time profiles.

Figure 8 shows the variation of the thus obtained axial dispersion coefficient with the superficial shell-side velocity. The axial dispersion coefficient increases with the shell-side velocity. The axial dispersion coefficient E_z obtained in the membrane module has intermediate values as compared to that of the pipe-flow and to the packed bed correlations (Wen and Fan, 1975). The presence of fibres in the module acts as the kind of packing and reduces the axial mixing and thus axial dispersion coefficient for membrane module is lower as compared to the pipe-flow correlation. Higher values of the axial dispersion coefficient for the membrane module as compared to packed bed correlation could possibly be explained by the fact that the membrane module contains two small empty zones at the inlet and the outlet of the module which contributes to the mixing of the shell-side fluid. In addition, the packing density of the fibres in the membrane module considered (around 20%) is much lower as compared to the packing density in packed beds (40–60%).

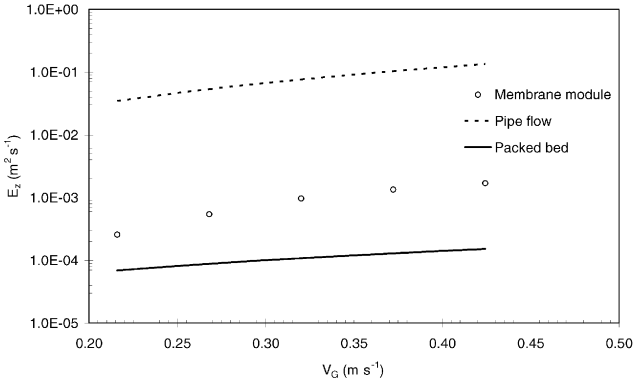

Figure 8. Effect of shell side velocity on axial dispersion coefficient.

For the single point tracer source at the inlet, a typical concentration profile of the tracer at the module exit is shown in Figure 9. The corresponding computed concentration profile is shown in Figure 10. The difference in the axes scale is due to the conversion of the module dimensions into cells and the conversion of the dimensionless outlet concentration into absolute values. Experiments were carried out at different shell-side velocities to study the effect of the shell-side velocity on the transversal dispersion coefficients.

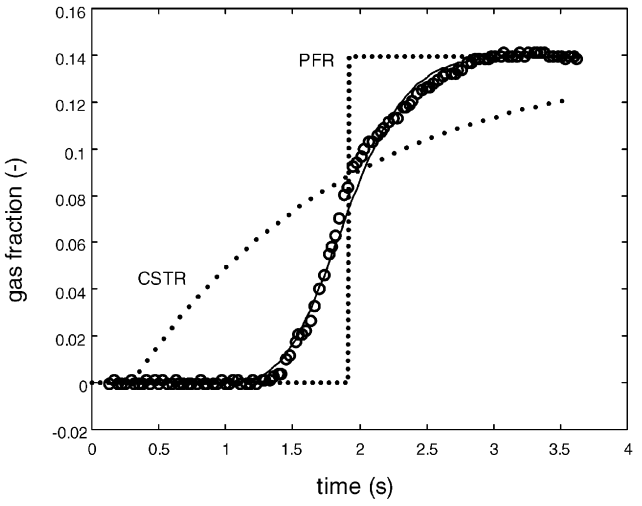

Figure 7. Typical response F-curve of rectangular hollow fibre membrane module (solid line indicates the axial dispersion model fit).

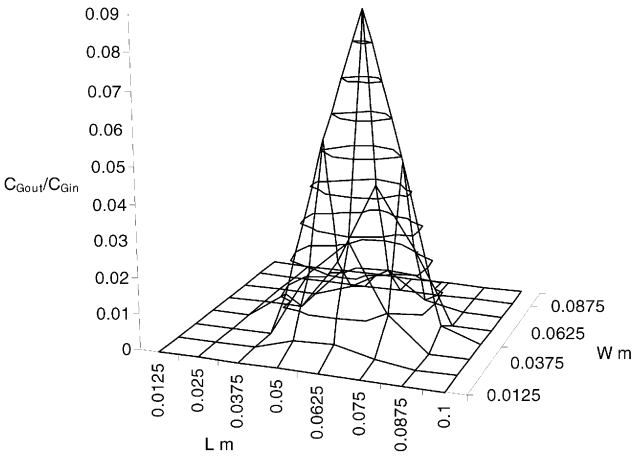

Figure 9. Measured concentration profile of the tracer at the exit of the module.

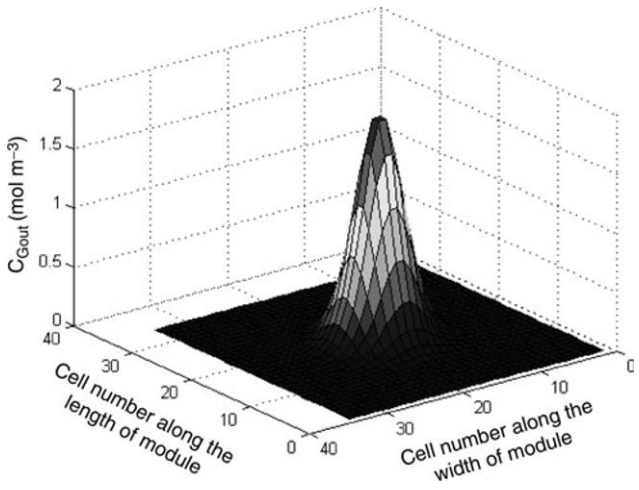

Figure 10. Computed concentration profile of the tracer at the exit of the module.

The variations of the obtained transversal dispersion coefficients with the shell-side velocity are given in Figures 11 and 12. In general, the transversal dispersion coefficients increase with the shell-side velocity. The transversal dispersion coefficient across the fibre length has a higher value and increases more strongly with the shell-side velocity when compared to the transversal dispersion coefficient along the length of fibre. This higher value and greater dependence of transversal dispersion coefficient across the fibre on the shell-side velocity can be attributed to the continuous splitting and remixing of the shell-side stream across each fibre. The axial dispersion coefficient E_z is much higher as compared to the transversal diffusion coefficients E_x and E_y. Similar observations were made for the packed bed and the pipe-flow dispersion coefficients (Westerterp *et al.*, 1984). This can be attributed to the increase in variance due to wall effects, especially at low L/D ratio. Relatively low values of the transversal dispersion coefficients indicates that at low shell-side flows little or no mixing present in the transversal direction and consequently important key factors such as heat transfer, mass transfer and mixing in transversal direction within the module are relatively poor.

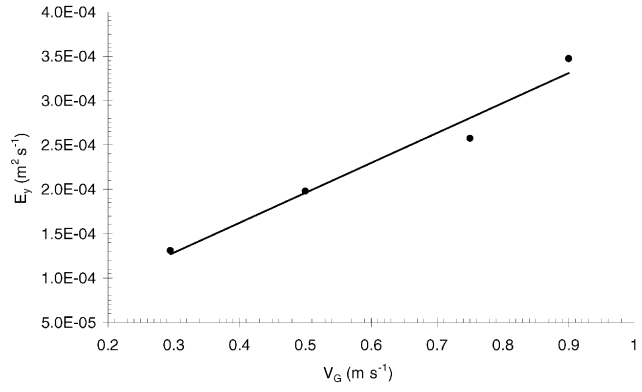

Figure 11. Transversal dispersion coefficient across the length of fibre.

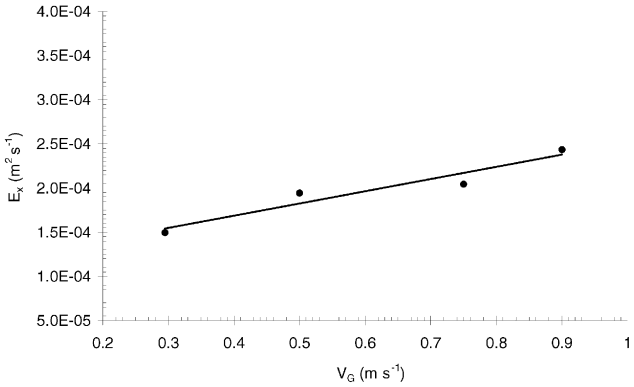

Figure 12. Transversal dispersion coefficient along the length of fibre.

CONCLUSIONS

In this work a novel ultrasonic technique is used to study the shell-side mixing behaviour of a cross-flow hollow fibre membrane contactor. The technique can be successfully used to characterize the system with low residence times typically in the range of 0.1 s. In addition, the technique can be also used to measure the local gas-phase concentrations gradients in the transversal or radial directions without disturbing the flow and thus can be successfully applied to characterize the flow bahaviour in complex geometries.

The shell-side mixing behaviour of a cross-flow hollow fibre membrane contactor is characterized in terms of dispersion coefficients in axial and transversal directions. Higher values of the axial dispersion coefficient and F-curve response indicate the non-ideal flow distribution on the shell-side of the module. Unlike parallel-flow hollow fibre membrane modules, strong by-passing of the shell side fluid is absent in the case of cross-flow hollow fibre membrane module. The axial dispersion coefficient is found to be in between the values obtained for pipe-flow and packed beds. The fibres used in the contactor act as a kind of packing and thus thereby reduce the mixing in axial direction. The axial dispersion coefficient is found to be higher than the transversal dispersion coefficients. The transversal dispersion coefficient across the fibre length has a stronger dependence on the shell-side velocity as compared to transversal dispersion coefficient along the fibre length due to the splitting and remixing action of the stream.

NOMENCLATURE

C	concentration, mol m^{-3}
D	diameter, m
$E(t)$	E-function defined in equation (6), s^{-1}
$F(t)$	F-function defined in equation (7)
E_v	bulk modulus of elasticity, Pa
E	dispersion coefficient, m^2 s^{-1}
L	length, m
MO_2	second moment, s^2
N	number of CSTR
P	pressure, pa
Pe	Péclet number ($Pe = \langle v \rangle$L/E)
t	time, s
$\bar{t}$	mean residence time, s
$\langle v \rangle$	average velocity, m s^{-1}
W	width, m

x distance, m
z length, m

Greek letters
Γ gamma function defined in equation (11)
Γ_{in} incomplete gamma function in equation (11)
ϕ tracer-gas volume fraction
ρ density, kg m^{-3}
θ reduced time defined in equation (9)
τ holding time, s
σ^2 variance defined in equation (10), s^2
σ_θ^2 normalized variance defined in equation (10)
ν sound velocity, m s^{-1}

Subscripts
ini initial condition
r reference component
v valve
x x-directional
y y-directional
z z-directional

REFERENCES

Brereton, C.M.H., Grace, J.R. and Yu, J., 1988, Axial gas mixing in a circulating fluidized bed, *Circulating fluidized bed technology II*, 307–315.

Cents, A.H.G., 2003, Mass transfer and hydrodynamics in stirred gas-liquid-liquid contactors, Ph.D. thesis, University of Twente, The Netherlands.

Chun, M. and Lee, K., 1997, Analysis on a hydrophobic hollow fibre membrane absorber and experimental observations of CO_2 removal by enhanced absorption, *Sep Sci and Tech*, 32(15): 2445–2466.

Danckwerts, P.V., 1953, Continuous flow systems: distribution of residence time, *Chem Engng Sci*, 2: 1–13.

Dahuron, L. and Cussler, E.L., 1988, Protein extraction with hollow fibres, *AIChE J*, 34(1): 130–136.

Feron, P.H.M., Jansen, A.E., Klaassen, R., Hanemaaijer, J.H. and ter Meulen, B.Ph., 1994, Membrane gas absorption processes in environmental applications, in *Membrane processes in separation and purification*, Crespo, J.G. and Boddeker, K.W. (eds) (Kluwer Academic, Dordrecht, The Netherlands), pp 343–356.

Lide, D.R. (ed.), 1999, *Handbook of Chemistry and Physics*, 79th edition (CRC Press, Boca Raton, FL, USA).

Karoor, S. and Sirkar, K.K., 1993, Gas absorption studies in microporous hollow fibre membrane modules, *Ind Eng Chem Res*, 32: 674–684.

Kreulen, H., Smolders, C.A., Versteeg, G.F. and van Swaaij, W.P.M., 1993, Microporous hollow-fibre membrane modules as gas–liquid contactors. Part 1. Physical mass transfer processes, *J Membr Sci*, 78: 197–216.

Mulder, M., 1996, *Basic Principles of Membrane Technology* (Kluwer Academic, Dordrecht, The Netherlands).

Nadeau, P., Berk, D. and Munz, R.D., 1996, Non-intrusive fast response concentration measurement device for chemical reactors, *Rev Sci Instrum*, 67: 847–853.

Oppenheim, A.V. and Schafer, R.W., 1989, *Discrete-time Signal Processing* (Pretence Hall Inc, New Jersey, USA).

Povey, M.J.W., 1997, *Ultrasonic Techniques for Fluids Characterization* (Academic Press, Amsterdam, The Netherlands).

Skelland, A.H.P., 1974, *Diffusional Mass Transfer* (John Wiley & Sons, New York, USA).

Seibert, A.F., Py, X., Mshewa, M. and Fair, J.R., 1993, Hydraulics and mass transfer efficiency of a commercial-scale membrane extractor, *Sep Sci & Tech*, 28(1–3): 343–359.

Viitanen, P.I., 1993, Tracer studies on a riser of a fluidized catalyst cracking plant, *Ind Eng Chem Res*, 32: 577–583.

Wang, Y., Chen, F., Wang, Y., Luo, G. and Dai, Y., 2003, Effect of random packing on shell-side flow and mass transfer in hollow fibre module described by normal distribution function, *J Membr Sci*, 216: 81–93.

Wen, C.Y. and Fan, L.T., 1975, *Models for Flow Systems and Chemical Reactors* (Marcel Dekker, New York, USA).

Westerterp, K.R., Van Swaaij, W.P.M. and Beenackers, A.A.C.M., 1984, *Chemical Reactor Design and Operation* (John Wiley & Sons, New York, USA).

Wickramasinghe, S.R., Semmens, M.J. and Cussler, E.L., 1992, Mass transfer in various hollow fibre geometries, *J Membr Sci,* 69: 235–250.

ACKNOWLEDGEMENTS

This research is part of the research program performed within the Centre for Separation Technology (CST), which is a co-operation between The Netherlands Organization for Applied Scientific Research (TNO) and the University of Twente. We also thank Benno Knaken for the construction of the experimental set up.

The manuscript was received 8 June 2004 and accepted for publication after revision 28 October 2004.